P.K. Sinha, et. al. International Journal of Engineering Research and Applications
www.ijera.com
ISSN: 2248-9622, Vol. 15, Issue 12, December 2025, pp 118-128

RESEARCH ARTICLE OPEN ACCESS

Calibration procedure for a pressure probe in non-null technique

P.K. Sinha[1], D. Chowdhury[2] A.Bagchi[3] and B. Majumdar[2]
[1] *Department of Mechanical Engineering, ICFAI University, Tripura – 799210, India.*
[2]*Department of Power Engineering, Jadavpur University, Kolkata – 700125, India.*
[3]*Department of Electrical Engineering, Dream Institute of Technology, Kolkata – 700104, India.*

Abstract
The analysis of fluid flow plays a crucial role in nearly all engineering applications. Accurate flow measurements—particularly of velocity, direction, and turbulence quantities—are essential for better understanding complex flow phenomena and for validating and refining computational flow models. Pressure probes are widely used for fluid flow measurements in both laboratory settings and industrial environments. In this study, a seven-hole pressure probe is calibrated using the non-null technique. An algorithm based on the non-null method is developed, which utilizes a calibration data database and applies a local least-squares interpolation technique to estimate flow properties. The non-null technique is found to offer advantages in terms of ease of use and improved accuracy in predicting flow measurement variables.
Keywords: seven-hole probe, non-null method, interpolation technique, regression model, sector scheme.

Date of Submission: 11-12-2025 Date of acceptance: 22-12-2025

Nomenclature

C_α	Pitch angle coefficient
C_β	Yaw angle coefficient
f_1, f_2, f_3, F(α), k	Calibration constants
G	Acceleration due to gravity(m/s^2)
U	Mean velocity (m/sec)
U_X	Velocity in x-direction (m/sec)
U_Y	Velocity in y-direction (m/sec)
U_Z	Velocity in z-direction (m/sec)
C_{Ptotal}	Total pressure coefficient
$C_{Pstatic}$	Static pressure coefficient
P	Pressure sensed by different holes
α	Pitch angle (°)
β	Yaw angle (°)
ρ	Density (kg/m^3)
ρ_m	Density of manometric fluid (kg/m^3)
ρ_{air}	Density of air (kg/m^3)
Subscripts	Hole numbers
1, 2, 3, 4, 5, 6, 7	
I	ith data point in a given sector
°	Degree
Superscripts	Average
¯	

I. Introduction

The seven-hole probe is a device used to measure pressure, designed to capture detailed data on all three velocity components of fluid flow, along with total and dynamic pressures. It has gained popularity because alternative methods—like five-hole probes and hot-wire anemometers—often struggle to deliver accurate results when the pitch and yaw angles go beyond ±30º. In contrast, the seven-hole probe maintains higher accuracy under these challenging conditions, making it especially valuable for analyzing complex three-dimensional flow fields.

To enhance sensitivity in detecting flow angularity, the seven-hole probe was introduced as an improvement over the five-hole pressure probe. It has demonstrated particular effectiveness in resolving intricate flow directions. Gallinton [1] provided a comprehensive account of the probe's development, calibration strategy, and interpolation method. Calibration involves aligning the probe at known flow angles and capturing pressure readings from all seven ports. A sectoring approach is then utilized to identify the calibration region by determining which port registers the maximum pressure. Within each defined sector, third-order polynomial equations are applied to relate flow characteristics to pressure coefficients and the probe's orientation. Gallinton's

calibration approach stands out for its originality and technical sophistication.

Everett et al. [2] made several advancements in the calibration process, simplifying the technique and enhancing its accuracy. Their method relies on third-order polynomial expressions derived from at least 20 calibration points, with angular intervals of 5º between each point. The calibration range extends to ±65º at Mach 0.88 and ±85º at Mach 0.20, with Reynolds number variations showing negligible effects on the calibration coefficients. There are various versions of the calibration procedure, primarily differing in the definition of pressure coefficients and the method of curve fitting. A limitation of using a single pressure coefficient definition is that it restricts the angular range within which the probe can provide reliable data, especially at high incidence angles where flow separation may occur over one or more of the pressure ports. To overcome this, Gerner and Maurer [3], and Gerner and Sisson [4], introduced a technique that splits the angular domain into low-angle and high-angle flow regions, a concept inspired by Bryer and Pankhurst's approach. This adaptation allowed for an extended usable cone angle of up to 70º, where the cone angle is defined as the angle between the velocity vector and the probe axis.

Gerner and Maurer [3] introduced separate non-dimensional pressure coefficients for pitch and yaw, each tailored to respond predominantly to its corresponding angle while minimizing interference from the other. These coefficients showed a linear relationship with their respective angles. As with all pressure coefficients, their values are also influenced by the Mach number, although this influence becomes relevant only in the compressible flow regime (Mach number > 0.3). Therefore, calibration data obtained at Mach numbers below 0.3 can be effectively used within the incompressible flow regime.

The polynomial fitting of non-dimensional coefficients to flow angles has been the subject of extensive study. Early approaches often utilized a global curve-fitting technique, where a single set of polynomials was applied to the entire calibration dataset, or a sector-based method, as seen in the work of Gerner and Maurer [3]. Rediniotis et al. [5] improved accuracy by dividing port-specific regions into smaller sections, increasing the number of regions and thus necessitating more localized polynomial models for the calibration coefficients. In contrast, Zilliac [6] proposed a local approach, in which the calibration database is searched, and interpolation or curve fitting is performed using only nearby data points. This method offered enhanced accuracy and greater flexibility, particularly for complex flow fields.

Zilliac [6] adopted the Akima interpolation method [7], a weighted-nearest-neighbors approach, as an alternative to the more traditional equally weighted curve-fitting technique. This shift led to a notable reduction in measurement errors. Furthermore, Zilliac introduced a simple yet effective strategy to detect and exclude pressure ports situated within flow-separated areas on the seven-hole probe, enhancing the overall reliability of the measurements.

Rediniotis and Vijayagopal [8] investigated the application of Artificial Neural Networks (ANNs) as an alternative to conventional polynomial curve fitting for correlating pressure coefficients with flow angles. Their method showed impressive predictive performance, especially in challenging flow scenarios.

Clark et al. [9] conducted a calibration study on hemispherical-tipped probes, covering a broad range of flow regimes, from high subsonic to Mach 2.0. They assessed five different definitions of calibration coefficients to determine the sensitivity to Mach number variations. Additionally, their work included a comparison of ten probes manufactured identically, highlighting the need for individual calibrations due to inherent variations introduced during the production process.

Takahashi [10] performed an in-depth analysis of coefficient behavior, emphasizing both the accuracy and the optimization of computational efficiency for real-time processing applications.

The ability of a five-hole or seven-hole probe to accurately resolve flow incidence angles is primarily determined by the probe's tip design and the arrangement of its pressure ports. In general, these probes can reliably measure flow angles up to about 70º. Gregory H. Johnson and Lawrence S. Reed [11] explored the performance of seven-hole probes in shear flow conditions, focusing on enhancing measurement accuracy in such environments. Their interpolation method facilitated the back-calculation of the apparent flow direction from the probe's measurements, enabling manual correction of inaccurate flow angles. This work also contributed to the development of surface-fit techniques for shear gradient corrections.

C. Venkateswara Babu et al. [12] proposed a hybrid calibration method that combined polynomial curve fitting with direct interpolation for seven-hole

probes. The probe was calibrated across a flow angle range of ±50º, with 9º intervals, and the measurement domain was divided into seven regions based on the port that recorded the maximum pressure. Within each region, calibration coefficients were calculated using a localized two-variable polynomial, fitted to the surrounding calibration data. The interpolation errors for flow angles were within ±1º, while the errors in total and static pressure were confined to within 0.5% and 1% of the dynamic pressure, respectively.

M.C. Gamerio Silva et al. [13] compared their direct interpolation method to the conventional interpolation approach. Their method utilizes linear interpolation directly on the dimensional coefficient matrices generated during the calibration process. They found that direct interpolation provided superior accuracy and greater result uniformity compared to the traditional method. Similarly, Espen S. Johansen and Rediniotis [14] developed a data reduction algorithm for non-nulling multi-hole pressure probes, applicable to both five-hole and seven-hole designs. Their method demonstrated an accuracy of ±0.6º for flow angles, with velocity predictions accurate to within ±1%, as reported in the literature.

Arnoud R.C. Franken and Paul C. Ivey [15] experimented with the rational function interpolation method, polynomial curve fitting, and neural networks for data reduction, using both four-hole cobra and pyramid probes. While they highlighted the advantages of neural networks, they did not provide a direct comparison between the methods. In contrast, Mathew D. Zeiger and Norman W. Schaeffler [16] developed a computational method to determine the alignment bias angles for multi-hole straight probes, including vertical bias angles, which are otherwise challenging to measure in cone-roll coordinates. Their method showed a difference of just 0.16º when compared to traditional techniques.

A. J. Pisascale and N. A. Ahmed [18] proposed a functional relationship based on theoretical considerations (potential flow), directly linking port pressures to flow properties. Their model proved highly accurate for determining large flow angles, with an error of less than 0.8º. Meanwhile, David Sumner [18] evaluated the data reduction techniques from Gallinton [1] and Zilliac [5] for calibrating a seven-hole conical pressure probe in incompressible flow. When applied to the same set of calibration data, both methods produced competitive results at low flow angles (below 30º), where the flow remained attached to the probe. Zilliac's direct interpolation method only outperformed Gallinton's technique at flow angles exceeding 30º. Sumner also noted that probe effectiveness diminished when the Reynolds number exceeded 5000.

For more complex flow fields, such as the wake behind a bluff body, where the angular range of flow direction exceeds the capabilities of five-hole or seven-hole probes, the omni-directional probe offers a valuable alternative. This probe extends the angular range of traditional probes, allowing accurate flow angle measurements up to 160º from its principal axis. Like the five-hole probe, the omni probe provides precise measurements of flow angles, local total and static pressures, and velocity magnitudes.

II. Experimental set up and algorithm for non- null method with sector scheme

Figure 1 illustrates the schematic diagram of the experimental setup used in this study. The setup consists of several key components: an air supply unit, a flow control system, a settling chamber, a contraction cone, and a straight test section. All components, except the air supply unit and the test section, were constructed from wood. The straight test section, made from transparent plexiglass, was designed to provide visual access. Calibration was carried out in the open jet of air exiting the test section, with ambient air serving as the working fluid.

For the calibration, a seven-hole hemispherical-tip pressure probe, shown in Fig. 2(c), was used. The probe is made up of seven stainless steel tubes, each having an outer diameter of 1.2 mm and an inner diameter of 0.9 mm. These tubes are securely glued together to form the complete probe assembly.

The seven stainless steel tubes are placed inside a jacket tube with a diameter of 4.16 mm. The probe's tip is shaped in a short L-configuration and filled with molten solder to form a hemispherical shape. Seven holes are drilled on the face of the hemispherical tip, with one hole at the center and the remaining six holes arranged symmetrically, each forming a 45º angle relative to the central hole. The probe itself is L-shaped, with the length of the 'L' measuring 4 mm. This short length helps minimize the blockage effect at the measurement point, reducing it to less than 3%. The overall length of the seven-hole pressure probe is 0.27 m.

The central hole (Hole 1) measures the reference pressure, which represents the stagnation pressure when the probe is aligned at 0º yaw. The pressure difference between the two horizontal holes (Holes 3 and 5) is used to calculate the yaw angle,

indicating the flow direction in the horizontal plane. Similarly, the pressure difference between the two vertical holes (Holes 2 and 4) reflects variations in the pitch angle. Generally, the pressure measured at the central hole is the highest among the seven, although this can vary depending on the flow angles.

The principle is most straightforward when considering changes in just one orientation—either horizontal (yaw) or vertical (pitch). To maintain brevity, this section will focus solely on the pressure variations for a decreasing yaw angle at zero pitch. The corresponding pressure changes for different orientations are summarized in Table 3.4 and can be further understood through the example provided below.

When the probe is rotated to a negative yaw angle and a positive pitch angle, hole 2 becomes more perpendicular to the flow, effectively acting as a larger obstruction. This leads to a decrease in flow velocity over hole 2's face and, as a result, an increase in pressure at hole 2. On the other hand, the flow velocity over hole 6 rises, causing a pressure drop at hole 6. As a result, the pressure difference (P_2 – P_6) increases. The opposite effect occurs when the yaw and pitch angles are reversed.

When the yaw angle becomes more negative, hole 2 begins to register stagnation pressure, while hole 6 captures static pressure. In cases where flow separation occurs at the probe's edge, a separation bubble could develop, causing significant fluctuations in the pressure readings at hole 6.

The calibration process for the seven-hole probe involves placing the probe at known angles relative to the flow and recording the pressures from all seven ports. From these measurements, dimensionless, velocity-invariant pressure coefficients are calculated by combining the differences between the recorded pressures. A sectoring method, shown in Fig. 3(b), is then employed to select the appropriate combinations of pressure coefficients, based on which port registers the highest pressure. This dynamic sectoring approach ensures precise measurements for flows with high angularity by adaptively selecting the most relevant pressure data.

In this study, compressibility effects were disregarded due to the flow velocity being limited to 40 m/s. However, the calibration method can be adapted for compressible flow regimes by including a dimensionless compressibility term in the calibration equations, as shown by Everett et al. [33]. The calibration process is carried out in two stages: the first stage focuses on low angles, where the central hole detects the maximum pressure, while the second stage addresses high angles, where the outer peripheral holes sense the maximum pressure.

2.1 Low Angles

At low flow angles, when the central hole detects the maximum pressure, the flow remains attached to all seven holes, without any separation or stalling. As a result, all seven pressure readings are utilized to determine the angular pressure coefficients, which exhibit a linear relationship with the flow angles. The three dimensionless pressure coefficients are defined as follows:

$$C_{P\alpha} = (P_4 - P_1) \Big/ (P_7 - P))$$
$$C_{Pb} = (P_5 - P_2) \Big/ (P_7 - P)$$
$$C_{Pc} = (P_6 - P_3) \Big/ (P_7 - P)$$
$$\overline{P} = (P_1 + P_2 + P_3 + P_4 + P_5 + P_6)/6$$

Only two of the three pressure coefficients are required to uniquely determine the orientation of the incoming velocity vector. However, if a pair of coefficients is chosen arbitrarily, the additional information from the third coefficient remains unused. As a result, the calibration equations are usually simplified to resolve a single pair of pitch and yaw components within a defined reference system.

$$C_{P\alpha} = (2C_{pa} + C_{pb} - Cp_{pc}) \Big/ \sqrt{3}$$
$$C_{P\beta} = (2C_{pb} + C_{pb} - Cp_{pc}) \Big/ 3$$
$$C_{PT} = (P_7 - P_T) \Big/ P_T - Ps)$$
$$C_{PS} = (P_S - \overline{P}) \Big/ (P_T - P_S)$$

When the flow angle surpasses around 30º—depending on the probe's geometry and manufacturing tolerances—the flow tends to separate on the lee side (downstream portion) of the probe. For a hemispherical probe tip, this separation typically occurs between 90º and 100º, as reported by Zilliac [6]. Under these conditions, the probe tip experiences a forward velocity component that remains attached to only four of the seven holes, while the remaining holes fall within the separated flow region, effectively stalling.

As a result, for high flow angles, the pressure coefficients are determined solely from the response of the four holes experiencing attached flow. Gallington [1] outlines the creation of twelve

dimensionless pressure coefficients, specifically designed for use at flow angles greater than approximately 20º.

Pressure coefficient for sector 1

*SECTOR*1

$$C_{P\alpha 1} = (P_1 - P_7) \Big/ P_1 - (P_2 + P_6/2)$$

$$C_{P\beta 1} = (P_6 - P_2) \Big/ P_1 - (P_2 + P_6/2)$$

$$C_{PT1} = (P_1 - P_T) \Big/ P_1 - (P_2 + P_6/2)$$

$$_{PS1} = (P_2 + P_6)/2 - P_S \Big/ P_1 - (P_2 + P_6/2)$$

Pressure coefficient for sector 2

*SECTOR*2

$$C_{P\alpha_2} = (P_2 - P_7) \Big/ P_2 - (P_1 + P_3/2)$$

$$_{P\beta_2} = (P_1 - P_3) \Big/ P_2 - (P_1 + P_3/2)$$

$$_{PT_2} = (P_2 - P_T) \Big/ P_2 - (P_1 + P_3/2)$$

$$_{PS_2} = (P_1 + P_3)/2 - P_S \Big/ P_2 - (P_1 + P_3/2)$$

Pressure coefficient for sector 3

*SECTOR*3

$$C_{P\alpha_3} = (P_3 - P_7) \Big/ P_3 - (P_2 + P_4/2)$$

$$_{P\beta_3} = (P_2 - P_4) \Big/ P_3 - (P_2 + P_4/2)$$

$$_{PT_3} = (P_3 - P_T) \Big/ P_3 - (P_2 + P_4/2)$$

$$_{PS_3} = (P_2 + P_4)/2 - P_S \Big/ P_3 - (P_2 + P_4/2)$$

Pressure coefficient for sector 4

*SECTOR*4

$$C_{P\alpha_4} = (P_4 - P_7) \Big/ P_4 - (P_3 + P_5/2)$$

$$_{P\beta_4} = (P_3 - P_5) \Big/ P_4 - (P_3 + P_5/2)$$

$$_{PT_4} = (P_4 - P_T) \Big/ P_4 - (P_3 + P_5/2)$$

$$_{PS_4} = (P_3 + P_5)/2 - P_S \Big/ P_4 - (P_3 + P_5/2)$$

Pressure coefficient for sector 5

*SECTOR*5

$$C_{P\alpha_5} = (P_5 - P_7) \Big/ P_5 - (P_4 + P_6/2)$$

$$_{P\beta_5} = (P_4 - P_6) \Big/ P_5 - (P_4 + P_6/2)$$

$$_{PT_5} = (P_5 - P_T) \Big/ P_5 - (P_4 + P_6/2)$$

$$_{PS_5} = (P_4 + P_6)/2 - P_S \Big/ P_5 - (P_4 + P_6/2)$$

Pressure coefficient for sector 6

*SECTOR*6

$$C_{P\alpha_6} = (P_6 - P_7) \Big/ P_6 - (P_5 + P_1/2)$$

$$_{P\beta_6} = (P_5 - P_1) \Big/ P_6 - (P_5 + P_1/2)$$

$$_{PT_6} = (P_6 - P_T) \Big/ P_6 - (P_5 + P_1/2)$$

$$_{PS_6} = (P_5 + P_1)/2 - P_S \Big/ P_6 - (P_5 + P_1/2)$$

2.2 Interpolation Procedure:

The interpolation method employs the pressure coefficients $C_{P\alpha}$ and $C_{P\beta}$ as independent variables to derive localized polynomial functions for determining dependent flow properties, such as pitch angle (α), yaw angle (β), total pressure (P_T), and static pressure (P_S). For each calculation point within a chosen sector, the interpolation process selects a polynomial that has been locally fitted using the surrounding calibration data.

For each sector, four response equations are formulated—one for each flow property (α, β, P_T, and P_S). Each flow property is expressed as a fourth-order polynomial expansion in terms of the pressure coefficients $C_{P\alpha}$ and $C_{P\beta}$. To determine the polynomial coefficients K_1 through K_{15} for each combination of flow property and sector, a least squares method is applied using all calibration data within the sector.

Overall, this approach results in a total of 28 polynomial functions and 42 calibration constants. The four flow properties are defined as follows:

$$\alpha_i = K_1,\alpha_i + K_{2,}\alpha_i \times C_{p\alpha,i} + K_{3,}\alpha_i \times C_{p\beta,i} + K_{4,}\alpha_i \times C^2_{p\alpha,i} + K_{5,}\alpha_i \times C_{p\alpha,i} \times C_{p\beta,i} + K_{6,}\alpha_i \times C^2_{p\beta,i} + K_{7,}\alpha_i \times C^3_{p\alpha,i} + K_{8,}\alpha_i \times C^2_{p\alpha,i} \times C_{p\beta} + K_{9,}\alpha_i \times C_{p\alpha,i} \times C^2_{p\beta,i} + K_{10,}\alpha_i \times C^3_{p\beta,i} + K_{11}\alpha_i \times C^4_{p\alpha,i} + K_{12,}\alpha_i \times C^3_{p\alpha,i} \times C_{p\beta,i} + K_{13,}\alpha_i \times C^2_{p\alpha,i} \times C^2_{p\beta,i} + K_{14,}\alpha_i \times C_{p\alpha,i} \times C^3_{p\beta,i} + K_{15,}\alpha_i \times C^4_{p\beta,i} \quad \ldots (1)$$

$$\beta_i = K_{1,\beta i} + K_{2,\beta i} \times C_{p\alpha,i} + K_{3,\beta i} \times C_{p\beta,i} + K_{4,\beta i} \times C^2_{p\alpha,i} + K_{5,\beta i} \times C_{p\alpha,i} \times C_{p\beta,i} + K_{6,\beta i} \times C^2_{p\beta,i} + K_{7,\beta i} \times C^3_{p\alpha,i} + K_{8,\beta i} \times C^2_{p\alpha,i} \times C_{p\beta,i} + K_{9,\beta i} \times C_{p\alpha,i} \times C^2_{p\beta,i} + K_{10,\beta i} \times C^3_{p\beta,i} + K_{11,\beta i} \times C^4_{p\alpha,i} + K_{12,\beta} \times C^3_{p\alpha,i} \times C_{p\beta,i} + K_{13,\beta i} \times C^2_{p\alpha,i} \times C^2_{p\beta,i} + K_{14,\beta i} \times C_{p\alpha,i} \times C^3_{p\beta,i} + K_{15,\beta i} \times C^4_{p\beta,i} \quad \ldots\ldots\ldots\ldots\ldots\ldots (2)$$

$$C_{pSi} = K_{1,Si} + K_{2,Si} \times C_{p\alpha,I} + K_{3,Si} \times C_{p\beta,i} + K_{4,Si} \times C^2_{p\alpha,i} + K_{5\,Si} \times C_{p\alpha,i} \times C_{p\beta,i} + K_{6,Si} \times C^2_{p\beta,i} + K_{7,Si} \times C^3_{p\alpha,i} + K_{8,Si} \times C^2_{p\alpha,i} \times C_{p\beta,i} + K_{9,Si} \times C_{p\alpha,i} \times C^2_{p\beta,i} + K_{10,Si} \times C^3_{p\beta,i} + K_{11,Si} \times C^4_{p\alpha,i} + K_{12,Si} \times C^3_{p\alpha,i} \times C_{p\beta,i} + K_{13,Si} \times C^2_{p\alpha,i} \times C^2_{p\beta,i} + K_{14\,Si} \times C_{p\alpha,i} \times C^3_{p\beta,i} + K_{15,Si} \times C^4_{p\beta,i} \quad \ldots\ldots\ldots (3)$$

$$C_{pTi} = K_{1,Ti} + K_{2,Ti} \times C_{p\alpha,i} + K_{3,Ti} \times C_{p\beta,i} + K_{4,Ti} \times C^2_{p\alpha,i} + K_{5,Ti} \times C_{p\alpha,i} \times C_{p\beta,i} + K_{6,Ti} \times C^2_{p\beta,i} + K_{7,Ti} \times C^3_{p\alpha,i} + K_{8,Ti} \times C^2_{p\alpha,i} \times C_{p\beta,i} + K_{9,Ti} \times C_{p\alpha,i} \times C^2_{p\beta,i} + K_{10,Ti} \times C^3_{p\beta,i} + K_{11,Ti} \times C^4_{p\alpha,i} + K_{12,Ti} \times C^3_{p\alpha,i} \times C_{p\beta,i} + K_{13,Ti} \times C^2_{p\alpha,i} \times C^2_{p\beta,i} + K_{14,Ti} \times C_{p\alpha,i} \times C^3_{p\beta,i} + K_{15,Ti} \times C^4_{p\beta,i} \quad \ldots\ldots\ldots (4)$$

Here, the superscript i corresponds to the selected sector, with i ranging from 1 to 7.

The final step involves determining the velocity components in three directions, as illustrated in Fig. 3(a). These components can be calculated using the following equations:

$$\overline{U} = \sqrt{(P_T - P_S) \times (\rho_m \times g \times 2/\rho_{air})}$$

$$\overline{U}_x = \overline{U} \times \cos\alpha \times \cos\beta$$

$$U_y = \overline{U} \times \sin\beta$$

$$U_z = \overline{U} \times \sin\alpha \times \cos\beta$$

A seven-hole pressure probe featuring a hemispherical tip (see Fig. 2) was utilized for the calibration procedure. This probe comprises seven stainless steel tubes—each with an outer diameter of 1.2 mm and an inner diameter of 0.9 mm—firmly bonded to form a single unit. The total length of the probe is 0.27 meters. To facilitate precise orientation, a custom-built traversing system was designed, allowing for rotation in both pitch and yaw directions [20]. For determining the calibration coefficients, the study employed a simple matrix regression method, following the approach outlined by Netter and Washerman [19].

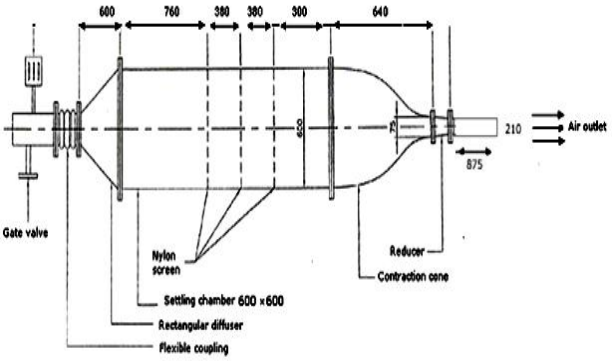

Fig.1. Schematic diagram of experimental setup

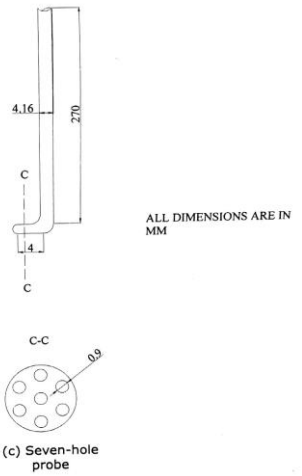

Fig.2. Schematic diagram of the pressure probe

The sector method divides the entire calibration domain into seven unique regions: one central region and six surrounding peripheral regions. Each zone is assigned based on the pressure reading from the individual holes—specifically, the zone is identified by the hole that registers the highest pressure. For example, if the central hole shows the peak pressure value, it is classified as zone 1. A comprehensive depiction of the probe and its corresponding zonal layout is provided in Fig. 3(a-b).

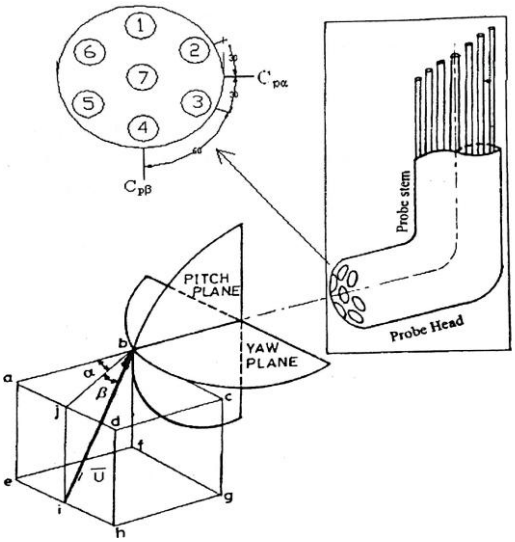

(a) Section view with hole nomenclature

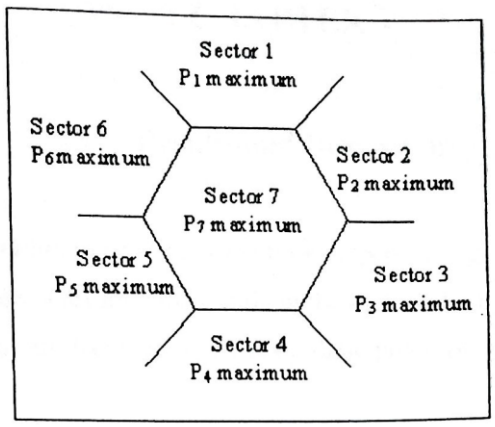

(b) Different sectors chosen

Fig.3. Sectoring scheme chosen for seven-hole probe (hole numbers 1to 7)

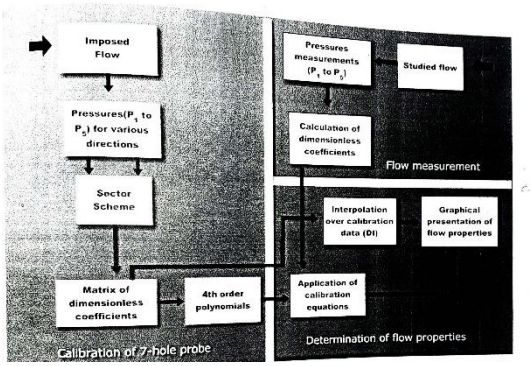

Fig.4. Flow chart of calibration/measurement process by
Seven-hole probe

$$\overline{U} = \sqrt{(P_T - P_S) \times (\rho_m \times g \times 2/\rho_{air})}$$

$$U_x = \overline{U} \times \cos\alpha \times \cos\beta$$

$$U_y = \overline{U} \times \sin\beta$$

$$U_z = \overline{U} \times \sin\alpha \times \cos\beta$$

III. Results and Discussions

This section discusses the calibration curves of key flow parameters—such as pitch angle, yaw angle, static pressure, and total pressure—obtained for a seven-hole probe using the non-null technique.

A flowchart is presented to illustrate the various steps involved in measuring flow properties using a seven-hole probe. The interpolation methods applied to estimate flow parameters from the probe data are compared against the directly measured values, allowing for a clearer assessment of interpolation accuracy and associated errors.

The seven-hole probe is calibrated using the sector method, which has the distinct advantage of extending the angular range over which the probe's performance remains relatively insensitive to changes in Reynolds number. Unlike the five-hole probe, which can be calibrated using the entire data set, this approach is not suitable for the seven-hole probe. This limitation arises because pressure readings from holes located in regions of separated flow may not accurately represent flow angles. Figure 4 presents a flowchart that outlines two non-null techniques—the 4OP and DI methods—used to analyze flow characteristics with the seven-hole directional pressure probe.

Figure 6 illustrates the α-β map, which displays the sectors identified during the calibration process. Each symbol on the map corresponds to the specific probe hole that recorded the highest pressure at a given flow angle. The naming convention for the holes is based on the orientation of the probe facing the incoming flow. As evident from the figure, each region of the α-β space is associated with a particular hole registering the maximum pressure, depending on the flow direction. This relationship forms the basis for determining the calibration constants. The pressure data were categorized into two angular regions: low-angle and high-angle. In the low-angle range, the central zone was primarily used, whereas in the high-angle range, the outer zones were considered. The recurring term "flow separation" becomes more intuitive through the visual representation; when the outer peripheral holes detect the maximum pressure, it indicates that the flow has separated from the probe surface.

Figures 5(a) through 5(g) display the α-β contour plots illustrating the pressure distribution recorded by each of the seven pressure ports (P1 to PT) on the probe. These contours reveal how pressure varies within the sectors where each port is dominant. The pressure distribution forms arc-shaped patterns, with pressure values increasing or decreasing depending on the flow angles (α and β), reflecting the directional sensitivity of the probe.

Figure 5(a) presents the α-β contour plot for pressure variations measured at Hole 1. This plot offers valuable insight into high-angle flow behavior. Notably, Hole 1 records the highest pressure when the probe is oriented at a pitch angle (α) of approximately 34º, while the yaw angle (β) remains within the range of -5º to +5º. The contour lines exhibit increasing curvature with rising pressure levels, indicating a corresponding decrease in local flow velocity at the probe surface, as per Bernoulli's principle.

Figure 5(b) illustrates the α-β contour plot showing pressure variations at Hole 2 when it registers the highest pressure relative to the other ports. The contour arcs appear non-symmetric, which can be attributed to minor geometric imperfections introduced during the manufacturing process. Hole 2 records peak pressure when the probe is aligned at a yaw angle (β) of approximately -30º, with the pitch angle (α) being greater than 0º.

Figure 5(c) presents the α-β contours where Hole 3 registers the maximum pressure compared to the other holes, corresponding to the mean flow velocity. Hole 3 experiences peak pressure when the probe is oriented with a pitch angle (α) ranging from -30º to 26º and a yaw angle (β) greater than or equal to -30º. At the specific orientation of α = -27º and β = -30º, Hole 3 measures the stagnation pressure, resulting in a minimum velocity across that hole.

Figure 5(d) displays the α-β contours where Hole 4 records the highest pressure relative to the other holes, reflecting the mean flow velocity. This plot illustrates how the pressure at Hole 4 varies with changes in α and β. Hole 4 senses maximum pressure when the pitch angle (α) ranges from -12º to +16º and the yaw angle (β) lies between -22º and -31º. At the specific orientation of α = -6º and β = -32º, Hole 4 registers the stagnation pressure, indicating minimal velocity at that point.

Figure 5(e) presents the α-β contours where Hole 5 records the highest pressure compared to the other holes, corresponding to the mean flow velocity. The plot illustrates how pressure at Hole 5 varies with changes in α and β. Hole 5 senses maximum pressure when the pitch angle (α) ranges from +14º to +32º and the yaw angle (β) lies between -32º and -10º. At the specific orientation of α = 24º and β = 26º, Hole 5 measures the stagnation pressure, indicating minimal velocity at that point.

Figure 5(f) depicts the α-β contours where Hole 6 registers the highest pressure compared to the other holes, corresponding to the mean flow velocity. This plot shows how the pressure at Hole 6 varies with changes in α and β. Hole 6 senses maximum pressure when the pitch angle (α) ranges from -7º to +37º and the yaw angle (β) lies between -32º and -22º. At the specific orientation of α = 12º and β = -26º, Hole 6 records the stagnation pressure, indicating minimal flow velocity at that position.

Figure 5(g) displays the α-β contours where Hole 7, located in the central zone of the probe, records the highest pressure relative to the other holes, corresponding to the mean flow velocity. Maximum pressure at Hole 7 occurs at low angles, with α ranging from -22º to +16º and β from -22º to +16º. The hole measures stagnation pressure when the probe is oriented at approximately α = -5º and β = 0º. Ideally, this stagnation point should be at α = 0º and β = 0º; however, slight manufacturing imperfections cause a shift, leading to this observed asymmetry.

Figures 5(a) through 5(f) illustrate the relationship between the yaw angle coefficient (C_{pyaw}) and the pitch angle coefficient (C_{ppitch}) for each sector. These plots show that the pitch angle (α) mainly depends on $C_{ppitch,}$ while the yaw angle (β) is primarily influenced by C_{pyaw}. As previously mentioned, zones 1 to 6 correspond to high flow angles, where unique combinations of C_{pyaw} and C_{ppitch} correspond to distinct values of α and β. The variations in these curves are utilized to interpolate flow angles during field measurements. Additionally, the data indicate that at higher flow angles, the difference between C_{pyaw} and C_{ppitch} is smaller compared to the center zone (low angles). The behavior of C_{pyaw} versus C_{ppitch} in the center zone (zone 7) closely resembles that observed in the central hole of the five-hole probe, as discussed earlier.

Figures 5(a) to 5(d) also display the variation of yaw angle against total pressure coefficient (C_{ptotal}) and static pressure coefficient ($C_{pstatic}$) for different pitch angles across zones 1 to 4. While C_{ptotal} and $C_{pstatic}$ can be interpolated over α and β, this method introduces errors since both angles are themselves derived via interpolation, propagating uncertainty. Therefore, as explained in Chapter IV, it is more accurate to interpolate $C_{pstatic}$ and C_{ptotal} directly from the yaw and pitch angle coefficients (C_{pyaw} and C_{ppitch}).

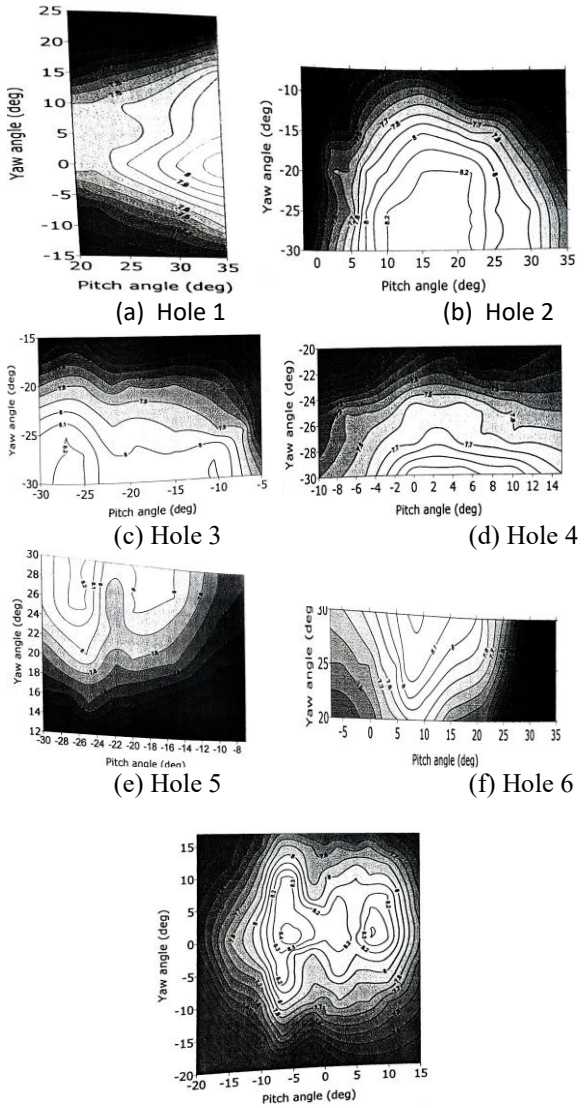

Fig.5. Pressure hole of Seven-hole probe response to pitch and yaw angle.

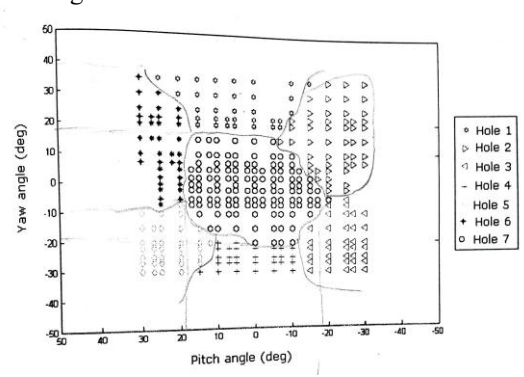

Fig.6. Sector map of pitch and yaw angle of seven-hole probe

Error:

To evaluate the errors associated with the fourth-order polynomial and direct interpolation methods, additional calibration data were collected for flow directions corresponding to intermediate points between the two angular grids. For these flow conditions—excluded from the calibration matrices—the flow characteristics were estimated using the two mentioned methods, with the pressures recorded by the seven probe holes serving as input. Since the actual flow characteristics were predefined, the error for each method could be determined by comparing the calculated results to the known (imposed) values.

Error distribution maps can be generated for each flow characteristic across all probe sectors, showing how the errors vary with the full range of incidence angles.

A comparison between the fourth-order polynomial (4OP) and direct interpolation (DI) methods was conducted by analyzing errors in pitch angle, yaw angle, static pressure coefficient, and total pressure coefficient relative to measured values. This evaluation focused on the center zone (Hole 7) and a peripheral zone (Hole 2). When comparing pitch and yaw angle errors in these two zones, both interpolation methods show comparable performance. For Zone 7, DI generally provides better accuracy in pitch angle interpolation than the 4OP method, with some exceptions—for example, at $\beta = -15^{o}$ and $\alpha = -10^{o}$, the 4OP method produced a more accurate yaw angle estimate than DI. In Zone 2, DI clearly outperforms 4OP in estimating both α and β.

Although the errors in pressure coefficients are very small (on the order of 0.01) for both methods, the 4OP occasionally yields better results than DI. Overall, either method is suitable for interpolation; however, 4OP is more time-consuming since it requires separate Fortran code development, whereas DI, implemented using MATLAB 7.0, allows direct interpolation from calibration data, making it less tedious and more convenient.

IV. Conclusion

Based on the results of the current study, the following conclusions can be drawn:

1. The calibration of the seven-hole probe employs the sector method, which offers the significant advantage of expanding the probe's angular range over which its response remains unaffected by variations in Reynolds number.
2. Of the two data reduction techniques evaluated, the direct interpolation method demonstrated superior performance compared to the fourth-order polynomial approach. This method achieved an accuracy of ±1° for both pitch and yaw angles, and ±1.5 m/s for velocity measurements.
3. The interpolation techniques applied to the seven-hole probe's flow property data were compared against directly measured values to better quantify and understand the associated errors.

References

[1]. Gallington R.W., "Measurement of very large flow angles with non-nulling seven-hole probes". *Aeronautic Digest* Spring/Summer (USAF Academy), 1980
[2]. Everest, K.N., Gerner, A.A., and Durston, D.A., 1982, "Theory and Calibration of Non- Nulling Seven-Hole Cone Probes for use in Complex Flow Measurement." AIAA paper 820232, AIAA *20th Aerospace Sciences Meeting*, Orlando, Jan.
[3]. Gerner, A.A. and Maurer, C.L., 1981, "Calibration of Seven-Hole Probe Suitable for High Angles in Subsonic Compressible Flows," United States Air Force Academy-TR-81-4.
[4]. Germer, A.A, and Sisson, G., 1981, "Seven-Hole Probe Data Acquisition System" United States Air Force Academy-TN-81-8, Nov.
[5]. Rediniotis, O.K. and Pathak, M.M. 1999, "Simple Technique for Frequency-Response Enhancement of Miniature Pressure Probes." AIAAJ, 37, no.7, PP. 897-899
[6]. Zilliac, G.G., 1989, "Calibration of Seven-Hole Probe for Ue in Fluid Flows with Large Angularity, " NASA Technical Memorandum 102200, Dec.
[7]. H. Akima, A method of bivariate interpolation and smooth surface fitting for irregularly distributed points, ACM Transactions on Mathematical Software 2 (4) (1978) 148.
[8]. Rediniotis OK, Vijayagopal R., (1999) Miniature multi-hole pressure probes and their neural-network-based calibration. AIAAI 37:666-674.
[9]. Clark, E.L., Henfling, J.F., and Aeschlimqn, D.P., 1992, "Calibration of Hemispherical-Head Flow Angularity Probes," AIAA Paper 92-4005, AIAA *17th Aerospace Ground Testing Conference,* Nashville, July.
[10]. Takahashi, T.T., 1997, "Measurement of Air Flow Characteristics Using Seven-Hole Cone Probes," NASA Technical Memorandum 112194, May.
[11]. Johnson G.H and Lawrence S.R., "Seven-hole probe in shear flow" American Institute of Aeronautics and Astronautics.
[12]. Babu, Venkatewara, C, Govardhan M, and Sitaram, N, 1998, "A method of calibration of a seven-hole pressure probe for measuring highly three dimensional flows," Meas. Sei. Feehnol., 9, pp. 468 – 476.
[13]. M.C.G. Silva, A.M.O. Lopes, C.A.C. Pereira, J.M.S. Cruz, "On the use of a linear interpolation method in the measurement procedure of a seven-hole pressure probe", Experimental Thermal and Fluid Science 28 (2003) 1 – 8.
[14]. Johonsen, E.S., Rediniotis, O.K., and Jones, G. 2001, "The Compressible Calibration of Miniature Multi-Hole Probes," ASME J, of Fluids Engineering, 123. Pp. 128-138.
[15]. Arnoud R.C. Franken and Paul C. Ivey, "Accelerating the Calibration of Multihole Pressure Probes by Applying Advanced Computational Methods", International Gas Turbine and Aero-engine Congress and Exhibition, Vienna, Austria, June 13 – 17, 2004, Paper No. 2004-GT-53434.
[16]. D.Z. Mathew and W.S. Norman, "Correcting multi-hole probe alignment bias errors post-calibration", American Institute of Aeronautics and Astronautics, 2001.
[17]. Pisasale A. J. Ahmed N.A., "Development of a functional relationship between post-pressures and flow properties for the calibration and application of multi-hole probes to highly three-dimensional flows". Experiment of Fluids 36 (2004) 422 – 436.
[18]. Summer D, "A Comparison of Data-Reduction Method for a Seven-Hole Probes,

the Journal of Fluids Engineering November 21, 2001.
[19]. Netter.J and Washerman.W, “Simple regression model in matrix
[20]. terms”, Applied linear Statistical Models, Richard D.Irwin, Inc, III, pp 200, 1975.
[21]. Chowdhury, D., "Modeling and calibration of pressure probes", M.P.E. Thesis, Jadavpur University, 2007